



**HAL**  
open science

## The new international reference system for pure alpha- and pure beta-emitting radionuclides and some electron capture decaying radionuclides by liquid scintillation counting

Romain Coulon, Ryszard Broda, Philippe Cassette, Sammy Courte, Aldo Dupire, Vincent Gressier, Simon Jerome, Steven Judge, Karsten Kossert, Haoran Liu, et al.

### ► To cite this version:

Romain Coulon, Ryszard Broda, Philippe Cassette, Sammy Courte, Aldo Dupire, et al.. The new international reference system for pure alpha- and pure beta-emitting radionuclides and some electron capture decaying radionuclides by liquid scintillation counting. *Journal of Radioanalytical and Nuclear Chemistry*, 2022, 331, pp.3221. 10.1007/s10967-022-08337-7 . cea-03776067

**HAL Id: cea-03776067**

**<https://cea.hal.science/cea-03776067>**

Submitted on 23 Sep 2022

**HAL** is a multi-disciplinary open access archive for the deposit and dissemination of scientific research documents, whether they are published or not. The documents may come from teaching and research institutions in France or abroad, or from public or private research centers.

L'archive ouverte pluridisciplinaire **HAL**, est destinée au dépôt et à la diffusion de documents scientifiques de niveau recherche, publiés ou non, émanant des établissements d'enseignement et de recherche français ou étrangers, des laboratoires publics ou privés.

1     **The new international reference system for pure alpha-**  
2             **and pure beta-emitting radionuclides**

3     Romain Coulon<sup>1</sup>, Ryszard Broda<sup>2</sup>, Philippe Cassette<sup>3\*</sup>, Sammy Courte<sup>1</sup>, Aldo Dupire<sup>1</sup>,  
4         Vincent Gressier<sup>1</sup>, Simon Jerome<sup>4</sup>, Steven Judge<sup>1\*</sup>, Karsten Kossert<sup>5</sup>, Haoran Liu<sup>6</sup>,  
5             Carine Michotte<sup>1</sup>, Manuel Nonis<sup>1</sup>

6     <sup>1</sup>*Bureau International des Poids et Mesures, Pavillon de Breteuil, F-92312 Sèvres Cedex,*  
7             *France*

8         <sup>2</sup>*National Centre for Nuclear Research Radioisotope Centre POLATOM, 05-400*  
9             *Otwock, Poland*

10        <sup>3</sup>*Université Paris-Saclay, CEA, List, Laboratoire National Henri Becquerel (LNE-*  
11            *LNHB), F-91120 Palaiseau, France*

12        <sup>4</sup>*Norges miljø- og biovitenskapelige universitet (NMBU), 1433 Ås, Norway*

13        <sup>5</sup>*Physikalisch-Technische Bundesanstalt (PTB), Bundesallee 100, 38116 Braunschweig,*  
14            *Germany*

15        <sup>6</sup>*National Institute of Metrology (NIM), 100029 Beijing, China*

16     \* *Now retired.*

17     E-mail address of the corresponding author: [romain.coulon@bipm.org](mailto:romain.coulon@bipm.org)

18             *Abstract*

19     The Bureau International des Poids et Mesures (BIPM) is developing with the support of  
20     national metrology institutes an extension to the existing international reference system  
21     of radionuclide metrology to address pure alpha-, pure beta-emitting and some electron  
22     capture-decaying radionuclides. The new service is based on a liquid scintillation counter

23 and the triple to double coincidence (TDCR) technique. A dedicated facility to prepare  
24 liquid scintillation sources and a TDCR system have been set up at the BIPM. The TDCR  
25 system was conceived and commissioned in order to ensure the long-term reproducibility  
26 of the reference it produces. The metrology is based on a dedicated approach which uses  
27 the TDCR value as a parameter to stabilize the output quantities of the system against  
28 changes in detection efficiency or asymmetry that could appear in a long-term period of  
29 operation. The quality assurance based on periodic controls of toluene-based liquid  
30 scintillation sources of  $^3\text{H}$  and  $^{14}\text{C}$  has permitted to demonstrate the reproducibility of the  
31 system for a 20-month period.

## 32 **Keywords**

33 Radionuclide Metrology, Key comparisons, Liquid scintillation, TDCR, ESIR

## 34 **1. Introduction**

35 The Bureau International des Poids et des Mesures (BIPM) operates an international  
36 reference system (the SIR) to compare standards of radioactivity realized by National  
37 Metrology Institutes / Designated Institutes (NMI/DIs), to enable NMI/DIs to  
38 demonstrate the equivalence of standards leading to a harmonized international  
39 measurement system. The operation of the international measurement system is described  
40 in more detail in a Mutual Recognition Arrangement, the CIPM MRA [1,2].

41 The SIR is a re-entrant ionization chamber; the output value is the ratio of the  
42 ionization current measured with the source to be analyzed to the current produced by  
43 long-lived sealed sources of  $^{226}\text{Ra}$  [3–5]. In practice, the long-term reproducibility and the  
44 precision achieved by this relative measurement allow to assess equivalences for most of  
45 the gamma-emitting radionuclides. To cope with the increasing demand in nuclear  
46 medicine in short-lived gamma-emitting radionuclides (e.g.  $^{99\text{m}}\text{Tc}$ ,  $^{18}\text{F}$ ,  $^{64}\text{Cu}$ ,  $^{11}\text{C}$ ...), a  
47 transportable version called the SIRTI is also available [6]. The well-type NaI(Tl)  
48 detector operates using as a reference: a long-lived sealed source of  $^{94}\text{Nb}$ . It is linked to

49 the SIR and can travel to laboratories far from the BIPM to obtain equivalences for these  
50 radionuclides. The main asset of the SIR/SIRTI services for NIM/DIs is to avoid  
51 organizing large-scale comparison exercises implying send radioactive sources around  
52 the world. The SIR is an on-demand service which permits the NIM/DIs to obtain  
53 equivalence whenever they desire. Moreover, the efficiency in delivering comparison  
54 results has been recently enhanced through a new database and automated reporting [7].

55 There are still some radionuclides that are not covered by the SIR/SIRTI services of  
56 the BIPM: pure (or quasi-pure) alpha-particle emitters, pure (or quasi-pure) beta-particle  
57 emitters, and some electron-capture decaying radionuclides (such as  $^{55}\text{Fe}$ ). The ionizing  
58 particles emitted during the decay of these radionuclides cannot pass (or very weakly)  
59 through the entry windows of the detectors and produce a sufficient signal. Meantime,  
60 there is an increasing demand to evaluate equivalence of radioactive standards containing  
61 these types of isotopes. New cancer treatments are emerging using radiopharmaceuticals  
62 tagged by radionuclides decaying in a way to deposit very locally the dose [8–10]. Hence,  
63 Targeted Beta-particle Therapy (TBT) and Targeted Alpha-particle Therapy (TAT) aim  
64 to efficiently damage cancerous cells while sparing healthy tissues. Radionuclides that  
65 are used (or studied to be used) in TBT are for instance:  $^{32}\text{P}$ ,  $^{89}\text{Sr}$ ,  $^{90}\text{Y}$ ,  $^{169}\text{Er}$ ,  $^{177}\text{Lu}$  and the  
66  $^{186}\text{Re}$ . Radionuclides that are used (or studied to be used) in TAT are for instance:  $^{225}\text{Ac}$ ,  
67  $^{211}\text{At}$ ,  $^{212}\text{Bi}$ ,  $^{212}\text{Pb}$ ,  $^{213}\text{Bi}$ ,  $^{227}\text{Th}$  and the  $^{223}\text{Ra}$ . Some of these isotopes, such as the  $^{177}\text{Lu}$   
68 used in the theragnostic perspective [11], emits enough x or gamma radiations to be  
69 measured by the SIR/SIRTI [12–14]. However, it is not possible for most of them. In  
70 addition to that, the need to assess the international equivalence of standards of pure  
71 alpha- or beta-emitting radionuclides arises also for environmental issues where for  
72 instance  $^{89}\text{Sr}$ ,  $^{90}\text{Y}$ ,  $^{160}\text{Tb}$ ,  $^{161}\text{Tb}$  and  $^{210}\text{Po}$  are of critical use for nuclear forensics [15–17].

73 Liquid scintillation counting appears to be the most suitable measurement techniques  
74 to address the measurement issue associated with these radionuclides. This is why, the  
75 extension of the SIR (called the Extended SIR (ESIR)) is under development since 2018  
76 and based on a liquid scintillation counter and an approach derived from the primary  
77 standardization technique called: Triple to Double Coincidence Ratio counting

78 (TDCR) [18,19]. On contrary to the SIR and SIRTl which achieve a long-term  
79 reproducibility using long-lived radioactive sources and a relative measurement, the  
80 ESIR implements another way to ensure reproducibility since the long-term stability of a  
81 liquid scintillation source cannot be assumed [20] even for the nonaqueous ones (see  
82 section 5). So, it has been decided to take benefit from the *TDCR* parameter which is  
83 strongly correlated with the detection efficiency of the system to realize a self-  
84 stabilization of the system. The output values delivered by the ESIR are comparison  
85 indicators,  $I$ , stabilized using the *TDCR* value in different ways such as:

- 86 •  $I_0$  is the non-stabilized comparison indicator,
- 87 •  $I_1$  is the comparison indicator stabilized by a 2<sup>nd</sup> order polynomial function of  
88 the *TDCR* value (built for robustness against efficiency changes),
- 89 •  $I_2$  is the comparison indicator stabilized by the calculation of an equivalent  
90 efficiency based on the TDCR model parametrized by fixed parameters (built  
91 for robustness against both efficiency and asymmetry changes),
- 92 •  $I_3$  is the comparison indicator obtain by making a monoenergetic assumption  
93 in the TDCR model (it can be used for isotopes emitting close-to-  
94 monoenergetic particles such as the  $^{55}\text{Fe}$ ).

95 Details on the calculation of these ESIR comparison indicators are given in [21–23].

96 In addition to this unique approach, it is also critical for this new service:

- 97 • to develop and maintain a source preparation facility with an accurate mass  
98 measurement of active solutions,
- 99 • to develop and maintain a TDCR system suitable for long-term operations,

- 100       • to develop and maintain a proper associated quality assurance to monitor the long-  
101           term reproducibility of the measurement system.

102

## 103           **2. The liquid scintillation source preparation facility**

104    To prepare liquid scintillation (LS) sources at the BIPM, aliquotes of an active solution  
105    standardized by a laboratory are injected into LS vials containing LS cocktail.

### 106                   *a. The liquid scintillation cocktail*

107    It was decided to use the Ultima-Gold (UG) cocktail from Perkin Elmer – (or equivalent).  
108    It permits to properly dissolve the aqueous active solution while providing a good  
109    scintillation yield. Ionisation quenching depends strongly on the properties of the LS  
110    cocktail and it cannot be assumed a perfect reproducibility from batch to batch of UG  
111    cocktails. However, as ionisation quenching effects are of relative minor importance for  
112    medium and high energy depositions into the LS liquid, it can be assumed that UG (or  
113    similar type of cocktails) will fit the purpose for the majority of radionuclides to address.

114    Nevertheless, the reproducibility of the ESIR when using UG cocktail could remains an  
115    issue for low energy-deposited particles encountered for instance during decays of  $^3\text{H}$ ,  
116     $^{63}\text{Ni}$ ,  $^{55}\text{Fe}$  or  $^{241}\text{Pu}$ . For these latter ones, the duration of key comparison exercises will be  
117    limited to the validity period of a given batch of UG. This option imposes constraints on  
118    laboratories as they cannot send their solutions when appropriate for them but only when  
119    a comparison is planned and during a limited period. The second option to ensure on-  
120    going comparisons as it is for the SIR, is to produce a specific LS cocktail at the BIPM  
121    under reproducible and sustainable conditions. A preliminary study has permitted, through  
122    a factorial design approach, to establish the preliminary composition of an LS cocktail  
123    that can be reproducibly realised at the BIPM. The components are notably chosen for  
124    not being impacted by the European REACH regulation. Thus, the diisopropylnaphthalen

125 entering as a solvent in UG composition is replaced by pseudocumen (1,2,4-  
126 trimethylbenzene) and the anionic surfactant 4-NPE is replaced by bis(2-  
127 ethylhexyl)hydrogene-phosphate. Also, to enhance the stability of the LS source in  
128 regards with the variation of PH of active solutions, the primary fluorophore 2,5-diphenyl  
129 oxazole (PPO) will be replaced by the more robust 1<sup>1</sup>,2<sup>1</sup>:2<sup>4</sup>:3<sup>1</sup>-terphenyle (p-terphenyle).  
130 Further studies will be realized to continue investigations on this option.

131 *b. The vials*

132 Glass vials will be the default type of vials used in the ESIR. However, as emphasis by  
133 the recent CCRI(II).Fe-55 comparison [24], polyethylene or frosted glass vials are better  
134 options to address <sup>55</sup>Fe and probably other radionuclides emitting low energy particles.  
135 Offering a better diffusion of photons in conformance with the TDCR model,  
136 polyethylene vials will be used for <sup>55</sup>Fe, <sup>63</sup>Ni, <sup>3</sup>H and <sup>241</sup>Pu.

137 *c. The balance*

138 The balance is a Mettler Toledo XPE26C set on a marble table (see Fig. 1). It is  
139 recalibrated each year by Mettler Toledo in compliance with the EURAMET calibration  
140 guide N°18 [25]. The standard uncertainty for metallic mass in the range from 1 mg  
141 to 100 mg is equal or better than 5 µg.



142

143

**Fig. 1** Photography of the BIPM balance

144 The differential weighing technique [26] is used to measure the mass of solution put in  
145 the vials. The active solution is transferred to a pycnometer which is measured before and  
146 after having released some droplets into the vials. One difficulty observed when weighing  
147 pycnometers is the electrostatic perturbation from the dielectric material. To cope this  
148 issue, a electrostatic discharger is set at the entrance of the balance to remove chages from  
149 the pycnomter. Also, prior to each source preparation, blank weighings (without droplet  
150 release) of the pycometer is realized to control that the reproducibility is contained within  
151 +/- 10  $\mu\text{g}$ .

152 The facility operates for producing LS sources of beta-emitting radionuclides but canot  
153 adress alpha-emitting radionuclides. Indeed, the handling of the latter is only allowed  
154 within a fume hood whatever the source activity is. The setup of a new balance in a fume  
155 hood is in project to enable alpha-emitting radionuclides to be adressed by the ESIR.

156

*d. The sources*

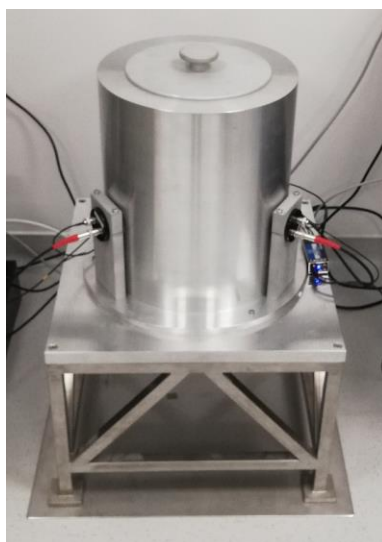
157 10 LS sources are realized for each ESIR submission. The amount of standard solution  
158 injected into each vials is calculated so that the double coincidence count rate  $r_D$  is

159 between  $5 \times 10^3 \text{ s}^{-1}$  and  $10^4 \text{ s}^{-1}$ . This constrain will guaranty to achieve a good counting  
160 statistic and to operate the system always in the same range of counting dead time.

161 It is important to note that it is asumed that the LS sources are not stable. So, it is stated  
162 in the procedure that the TDCR measurements must be done within the week just after  
163 the source preparation.

### 164 **3. The TDCR system**

165 The TDCR system of the ESIR is presented in Fig. 2.



166

167 **Fig. 2** Photography of the ESIR TDCR system

168 As any TDCR system, it is composed of:

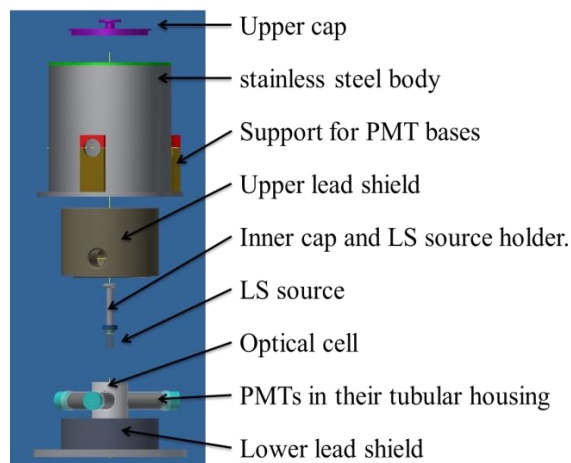
- 169 • a mechanical structure,
- 170 • an optical cell,
- 171 • a photo-conversion device using 3 photomultiplier tubes (PMTs),
- 172 • a specify signal processing electronics.

173 Technological options for these elements must be specified to address long-term  
174 reproducibility and maintainability. To this end, an effort is made to maximize the  
175 detection efficiency (close to 1) to minimize the part of the method in the long-term  
176 reproducibility strategy. This property is particularly of importance for isotopes emitting  
177 low energy particles such as  $^3\text{H}$ ,  $^{63}\text{Ni}$ ,  $^{55}\text{Fe}$ ,  $^{241}\text{Pu}$  because the model from which  $I_1$ ,  $I_2$  and  
178  $I_3$  were conceived comes close to its limits to describe the underlying physics due notably  
179 to low photoconversion statistics, significance of the ionization quenching, delayed  
180 fluorescence, etc. Also, materials and electronics must be chosen in a way to guaranty the  
181 sustainability of the reference produced by the system even when parts of the equipment  
182 are damaged or come to obsolescence.

183 *a. The mechanical structure*

184 Unlike many TDCR systems, it was chosen not to implement a fourth gamma-rays  
185 channel or an embedded source of  $^{241}\text{Am}$  for Compton coincidence feature. These options  
186 gives the possibility of performing  $4\pi(\text{LS})\beta\text{-}\gamma$  counting [27] or Compton source  
187 efficiency tracing [28]. Another TDCR system will be dedicated for these options  
188 because it is preferable for the ESIR to simplify the design as much as possible to meet  
189 our specific need exclusively. Thus, the absence of a fourth gamma-rays channel permit  
190 to setup a 10 cm-thick gamma-rays shielding with a greater spherical coverage and  
191 therefore a lower background noise. Also, the implementation of an  $^{241}\text{Am}$  sealed source  
192 for Compton coincidence requires coring a collimator hole through the optical cell. The  
193 absence of this feature optimizes the symmetry ( $120^\circ$  angular spacing between PMTs) of  
194 the system. This optimizes the relevance of the  $I_1$  indicator (not implementing asymmetry  
195 correction) and minimizes the stabilization effort carried out by the  $I_2$  comparison  
196 indicator to maintain reproducible output values under possible asymmetry.

197 The assembly is placed on a reinforced support and incorporated into a cylindrical steel  
198 cover ensuring light tightness. All this mechanical structure was designed and machined  
199 at the BIPM workshop. Fig. 3 shows the exploded view of the BIPM TDCR system.



200

201

**Fig. 3** Exploded view of the BIPM TDCR system

202

*b. The optical cell*

203

204

205

206

207

208

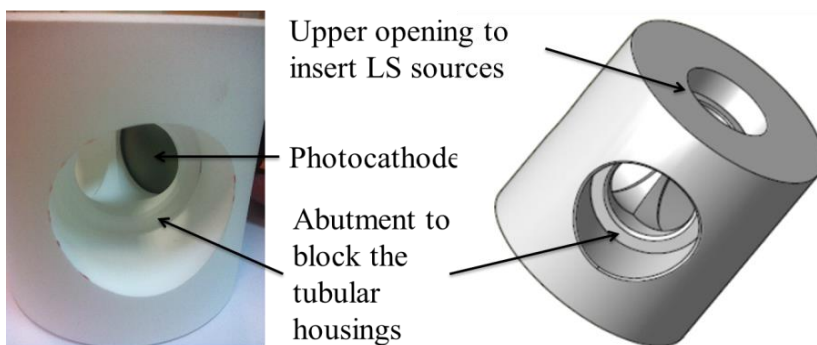
209

210

211

It was decided to machine the optical cell in low density PTFE (Gigahertz-Optik ODM98-B [29]). This material, used by the PTB in one of their TDCR systems, has a very good reflectivity (98%) for visible photons. Moreover, this material is also known for its great immunity to chemical attacks and to radiation damages [30]. Therefore, it gives the TDCR system a greater long-term stability of the optical properties than traditional painting of titanium oxide, which requires to be periodically renewed. The optical cell (presented in Fig. 4) has been machined at the BIPM workshop. Like the photocathodes, the internal surfaces of the optical cell are frosted to maximize the stochastic scattering of photons in accordance with the TDCR model.

212



213 **Fig. 4** Photography and 3-D drawing of the optical cell

214 *c. The photoconversion device*

215 The insertion of PMTs through the shield to reach the optical cell is a delicate point  
216 where light leaks can occur. To cope with this problem, a tube adjusted to the diameter of  
217 the tubular housings of the PMTs has been conceived (see Fig. 5a). This tube comes to  
218 lock in abutment of the optical cell so that the photocathode penetrates therein. The PMT  
219 is fixed in the tubular housing thanks to an O-ring (see Fig. 5b).



220

221

(a)

(b)

222 **Fig. 5** Tubular housing of PMT tubes. (a) with a PMT inserted; (b) empty housing  
223 showing the O-ring

224 The PMTs are Hamamatsu R331-05 selected to have an identical quantum efficiency of  
225 +/- 1 % for an excitation at the wavelength of 420 nm. As can be seen in Fig. 5a, the  
226 bialkali photocathodes are curved and frosted in order to respectively maximize the  
227 optical efficiency and the stochastic diffusion of fluorescence photons. The curvature  
228 allows the photocathode to approach the LS source borders within 2 mm. Furthermore,  
229 the window material is low K content to minimize background noise. Before being  
230 inserted into its tubular housing, the PMT is covered with a mu-metal foil to limit the  
231 impact of possible electromagnetic disturbances on electron multiplication. The cathode  
232 is polarized with a positive voltage. And, in accordance with our strategy to avoid

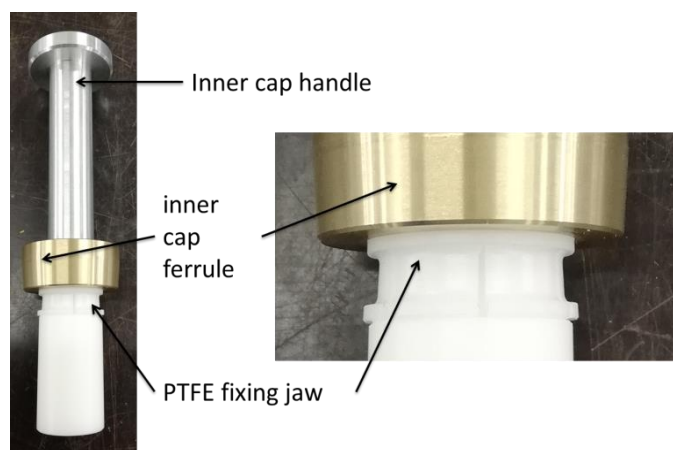
233 dispensable features which could be sources of disturbance for the reference to be  
234 produced, no potentiometric defocusing has been implemented.

235 *d. The LS source positioning system*

236 The previous BIPM TDCR system used an extruded base at the bottom of the cell to  
237 position the source. This approach turns out to have the following two disadvantages:

- 238 • having a LS source off-center from the axis of the photocathodes that is not  
239 optimal to maximize the detection efficiency,
- 240 • achieving in practice mediocre reproducibility of the positioning of the LS  
241 source.

242 For the new system, a special plug has been designed to hold the LS source in a  
243 reproducible position maximizing the detection efficiency. The source volume is  
244 maintained in the axis of the photocathodes using a jaw build in PTFE which grab the  
245 caps of the LS vials (see Fig. 6). This approach is implemented within POLATOM's  
246 TDCR systems and gives hope for an almost perfect reproducibility of the positioning of  
247 the source.



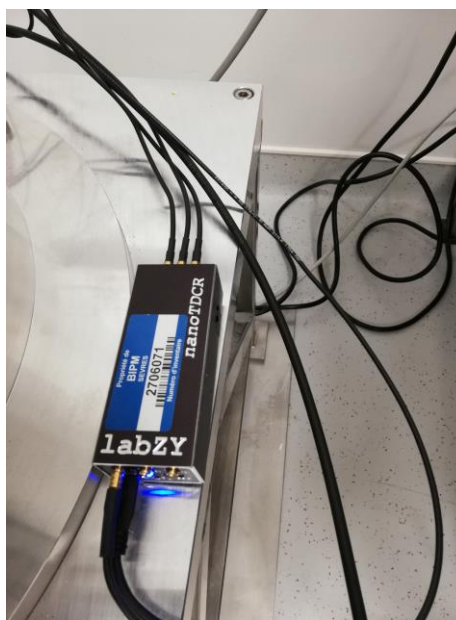
248

249 **Fig. 6** Photography of the inner cap of the BIPM TDCR system handling a LS source

250 *e. The electronics*

251 The PMTs are polarized at a voltage equal to +2500 V using NHQ103M HV units. This  
252 voltage value is ideal to enable the system to detect properly single photoelectron events.  
253 The anode signals from the three PMTs are processed by the nanoTDCR module [31,32]  
254 (see **Fig. 5**). It embeds in its FPGA the same extended dead time processing as in the  
255 reference MAC3 unit [33] which is unfortunately no more maintained. The nanoTDCR  
256 provides the following quantities:

- 257
- the triple coincidence count rate  $r_T$ ,
  - 258 • the logical sum of the double coincidence count rate  $r_D$ ,
  - 259 • the double coincidence count rates  $r_{AB}$ ,  $r_{BC}$ ,  $r_{AC}$  of each pair of the three channels  
260 A, B and C.
  - 261 • the count rates  $r_A$ ,  $r_B$ ,  $r_C$  from channels A, B and C.



262

263 **Fig. 7** Photography of the nanoTDCR module

264 The key comparison indicators of the ESIR are built from these quantities such as:

- 265
- $I_0$  only uses  $r_D$ ,
  - 266 •  $I_1$  uses  $r_D$ , the *TDCR* value,  $R_T/R_D$ , plus two preset parameters  $\alpha_1$  and  $\alpha_2$ ,

267 •  $I_2$  uses  $r_D$  and the TDCR values,  $R_T/R_{AB}$ ,  $R_T/R_{BC}$ ,  $R_T/R_{AC}$ , plus preset parameters  
268 for the TDCR model: the Birks constant  $k_B$ , the stopping power  $dE/dx(E)$  and the  
269 energy spectrum  $S(E)$ ,

270 •  $I_3$  uses  $r_T$ ,  $r_{AB}$ ,  $r_{BC}$ ,  $r_{AC}$ .

271 The count rates  $r_A$ ,  $r_B$ ,  $r_C$  are used to correct the measurement from accidental  
272 coincidences [34]. Details are available in [35].

273 To enhance the long-term maintainability of the ESIR, a redundant electronic based on  
274 the CEAN digitizer DT5730S is planned to be setup. The list mode data acquisition will  
275 permit to have more control on the algorithmic implemented for the TDCR signal  
276 processing.

#### 277 **4. Commissioning of the TDCR system**

278 The ESIR aims to produce a fixed reference. So it is of importance that parameters used  
279 in the signal processing are defined once and for all. The extended dead time algorithm  
280 requires the following parameters:

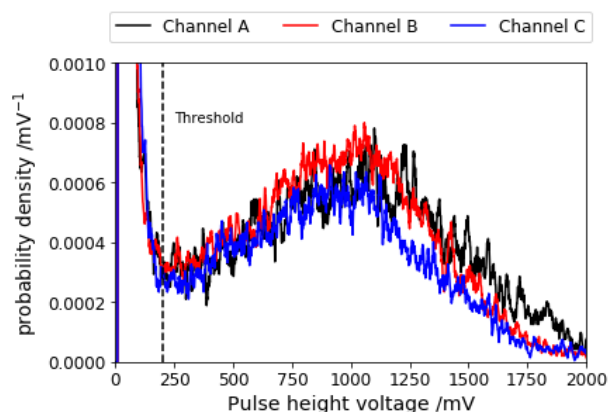
- 281 • The discrimination thresholds on each channel,
- 282 • The extended dead time period,
- 283 • The coincidence resolving time.

284 One interesting feature of the nanoTDCR is to process the signal with two different  
285 extended dead times and two different resolving times. The setup of these signal  
286 processing parameters is described below.

##### 287 *a. Setup of the discrimination thresholds*

288 Fig. 8 presents the pulse high spectra recorded without LS sources in the TDCR system.  
289 The left component comes from the thermal electronic noise and the spread peak centred

290 on about 1 V is induced by the dark noise related to the stochastic thermionic emission  
291 from photocathodes. The three spectra as almost superimposed which means that PMTs  
292 displayed equivalent thermal noise magnitude and voltage gain. The first set step is to set  
293 the discrimination threshold in the valley of the spectra in order to maximize the signal to  
294 noise ratio, i.e., minimizing the thermal noise impact while maximizing the detection  
295 probability of single electron pulses. According to the shape observed in Fig. 6,  
296 thresholds are therefore set at -200 mV for all the 3 channels A, B and C.



297

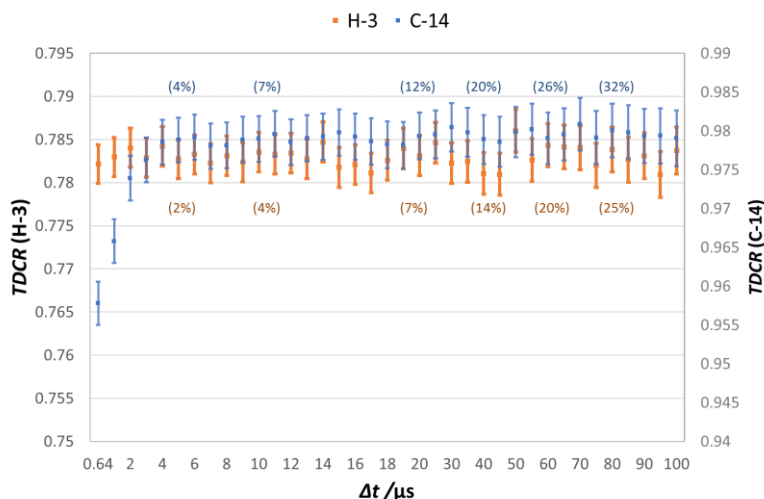
298 **Fig. 8** Pulse high spectra of single photoelectron pulses from the three channels of the  
299 TDCR system

300 *b. Setup of the extended dead time*

301 After-pulses induce a metrological challenge in every measurement systems  
302 implementing PMTs [36]. To limit after-pulses impact, the extended dead time method  
303 paralyzes the signal processing during an imposed period  $\Delta t$  after each triggering  
304 occurring on one of the three channels.

305 Considering a resolving time set to 50 ns, the TDCR value was estimated as a function of  
306 the extended dead time period  $\Delta t$  for 2 toluene-based standard sources of  $^3\text{H}$  (3.2 kBq)  
307 and  $^{14}\text{C}$  (2.0 kBq) and presented in Fig. 9. The influence of after-pulses on the  
308 measurement seems to be a function of the energy of the beta particles and therefore of  
309 the amplitude of the primary pulse. No significant impact is observed in the case of  
310 tritium and a  $\Delta t$  of 5  $\mu\text{s}$  seems sufficient for  $^{14}\text{C}$  sources to filter this type of disturbance.

311 To maximize the statistical precision of the counting and the accuracy of the live-time  
 312 estimation, the dead time of the measurement must be minimized. Thus, by taking a  
 313 reasonable safety margin, a first  $\Delta t$  equal to 10  $\mu\text{s}$  will ensure after-pulse filtering while  
 314 minimizing the dead time. The second  $\Delta t$  is set equal to a larger value, 50  $\mu\text{s}$ , and will  
 315 permit to compare measurement results obtained with these two paralyzing times to  
 316 assess the impact of after pulses.



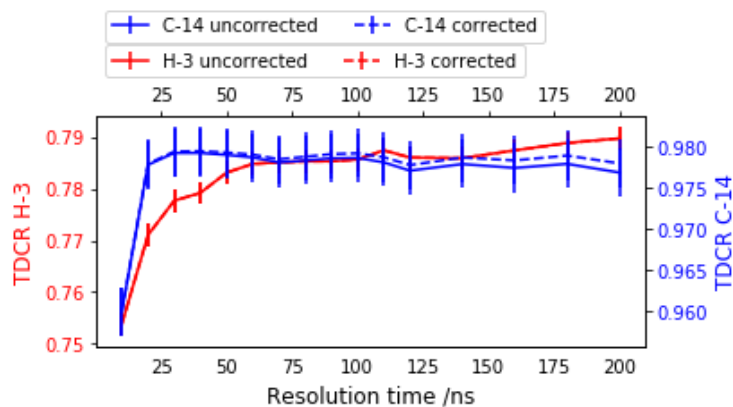
317

318 **Fig. 9** *TDCR* value as a function of the extended dead time for the two sources of  $^3\text{H}$  and  
 319  $^{14}\text{C}$ . The measurement dead time is displayed in brackets.

320 *c. Setup of the coincidence resolving time*

321 The resolution time  $\Delta\tau$  is the time window during which any triggering between the two  
 322 or three channels will be considered as a double or triple coincident event. Too short a  $\Delta\tau$   
 323 leads to a risk of non-detection. Conversely, too long a resolution time increases the risk  
 324 of accidental coincidences. Keeping the same experimental configuration as before, the  
 325 evolution of the *TDCR* value as a function of the resolving time is studied. It is observed  
 326 in Fig. 10 a disparity of behaviour between  $^3\text{H}$  and  $^{14}\text{C}$  with the resolving time. While the  
 327 *TDCR* value of  $^{14}\text{C}$  reaches a constant (or slightly decreasing) value from a resolution  
 328 time greater than 30 ns, the *TDCR* value associated with  $^3\text{H}$  increases monotonically.  
 329 This can be explained by the fact that the stopping power of very low energy electrons is

330 greater than for higher energy electrons. The decays of tritium nuclei will therefore have  
331 a greater tendency to produce triplet states of excitement leading to delayed fluorescence  
332 or phosphorescence [37]. Anyway, this phenomenon depending on the scintillating  
333 liquid, concerns almost exclusively low energy emitting isotopes such as  $^{55}\text{Fe}$  or tritium.  
334 Although it can potentially cause a bias in the context of primary measurements, these  
335 biases are constant for a given scintillator and can therefore be assumed in ESIR  
336 operation. So, a value of  $\Delta\tau$  equal to 50 ns will be considered whatever the radionuclide  
337 is. This choice guarantees a margin compared to the minimum of 30 ns observed here and  
338 greatly minimizes the risk of accidental coincidence. A measurement with a resolution  
339 time of 100 ns will also be simultaneously recorded in order to control the stability of the  
340 scintillating liquid with respect to the phenomenon described above.



341

342 **Fig. 10** TDCR value as a function of the coincidence resolving time for the two sources  
343 of  $^3\text{H}$  and  $^{14}\text{C}$ .

### 344 5. The quality assurance

345 The quality assurance will play a critical role to control the long-term reproducibility of  
346 the reference values produced by the ESIR. A set of procedures were established and  
347 specific attention was carried on the automation of the measurement analysis by a Python  
348 program and by establishing a Git-controlled database in the same framework as it was  
349 recently established for the SIR [7].

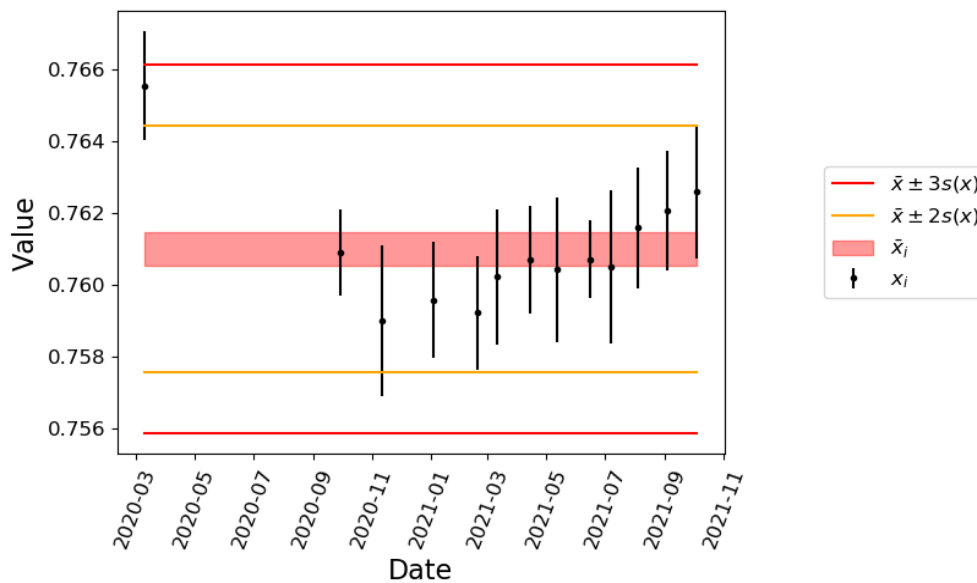
350 Besides, a monthly periodic control of the system was setup since its commissioning in  
351 August 2020. The check sources are 6 toluene-based LS sources ( $^{14}\text{C}$  sources and  $^3\text{H}$   
352 sources) known for their good stability over a long-term period. The reproducibility of  
353 the ESIR is assessed by performing statistical analysis on these quality measurements. As  
354 recommended by the ISO17025:2017, control charts (x-chart, R-chart, CUSUM chart and  
355 EWMA chart) are applied to detect outliers or drifts signaling that the system is not under  
356 statistical control. Also, the consistency of the data set with the uncertainty evaluation of  
357 each point is tested using a Chi-squared test.

358 The results for one of the tritium sources for which a first measurement point was  
359 obtained in March 2020 are displayed in Figs. 11-14. The error bars are standard  
360 uncertainty associated with the measurement points,  $x_i$ . The lower and upper control  
361 limits are the mean of all the measurement points  $\pm 2$  times (yellow lines) or 3 times  
362 (red lines) standard deviation (type A evaluation). The central red line represents the  
363 mean with a thickness equal to  $\pm 1$  standard deviation of the mean value.

364 The raw comparison indicator  $I_0$  and the  $TDCR$  values (Figs. 11 and 12) show clearly that  
365 the system is not by itself stable. Even if the raw measurement data  $I_0$  passes tests from  
366 control charts, it fails the Chi-squared test with a p-value equal to 0.002 (corresponding to  
367 a Birge ratio equal to 1.76). So, the hypothesis of consistency of the measurements  
368 according to their individual uncertainty evaluations can be rejected with a 95 %  
369 confidence level. This means that it exists slight (about 0.2 %) but significant drifts in the  
370 detection efficiency that are not taken into account in the uncertainty budget.

371 For the same data set, key comparison indicators  $I_1$  and the  $I_2$  are displayed  
372 in Fig. 13 and Fig. 14. They both pass tests from control charts and the Chi-squared test  
373 with p-values close to 1. This result stresses the robustness provided by the approach  
374 developed for the ESIR. It demonstrates that the ESIR is capable to provide reproducible  
375 values  $I_1$  and  $I_2$  during a period of 20 months.

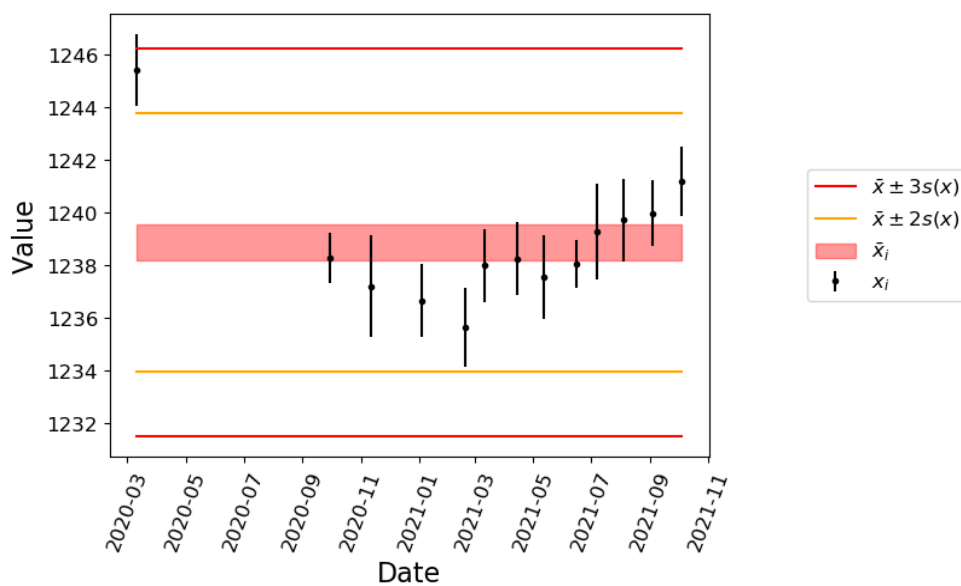
376



377

378

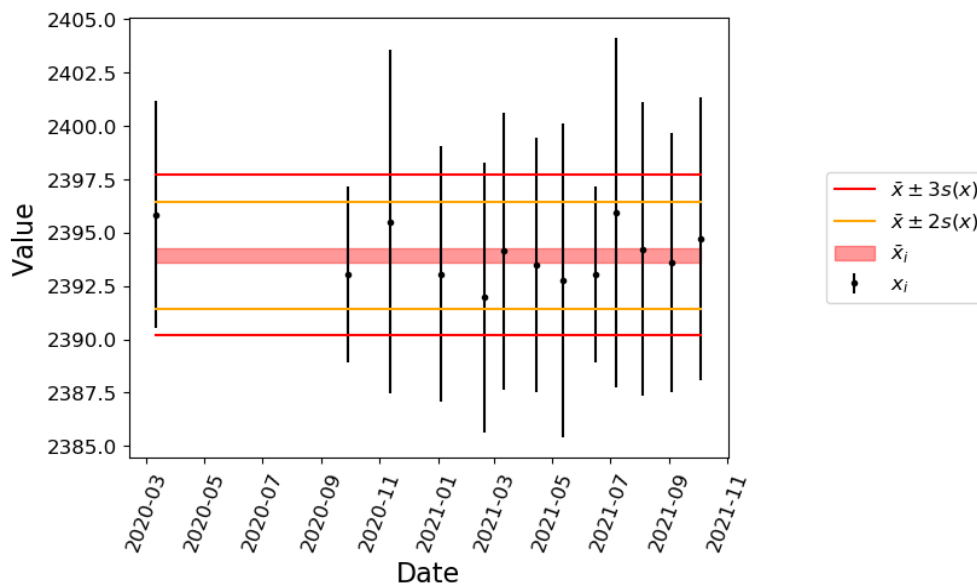
**Fig. 11** TDCR values obtained for the  $^3\text{H}$  source HDCO since March 2020



379

380

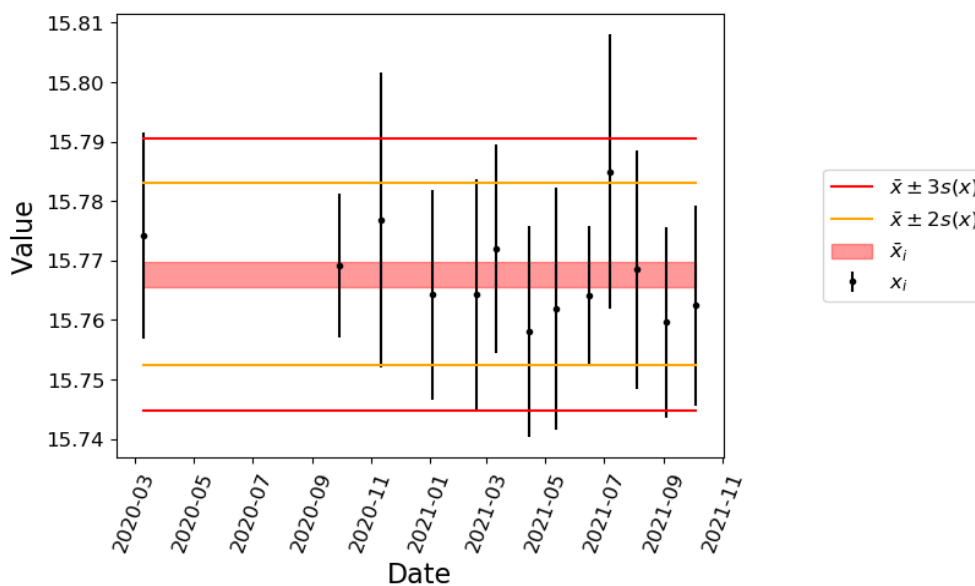
**Fig. 12**  $I_0$  values obtained for the  $^3\text{H}$  source HDCO since March 2020



381

382

**Fig. 13**  $I_1$  values obtained for the  $^3\text{H}$  source HDCO since March 2020



383

384

**Fig. 14**  $I_2$  values obtained for the  $^3\text{H}$  source HDCO since March 2020

385

Results for the other check standards are available as supplementary information.

386

387        **Conclusions**

388    A liquid scintillation source facility and a new TDCR system have been set up at the  
389    BIPM to extend the SIR to pure alpha-, pure beta-emitting and some electron capture-  
390    decaying radionuclides. The objective is to improve the traceability chain for  
391    radionuclides of interest for new cancer treatments and some environmental issues.

392    The service was commissioned in August 2020. Since this date, the ESIR operates,  
393    through a set of procedures and fixed defined parameters, to produce highly reproducible  
394    measurement quantities. These quantities called key comparison indicators will permit to  
395    establish reference values (KCRV) for these radionuclides and degrees of  
396    equivalence for the participating NMI/DIs. The ESIR aims to be an on-demand service  
397    for at least isotope emitting medium and high energy particles. A CCRI(II) pilot study on  
398    Co-60 key comparison is underway to validate the ESIR against the SIR in the context of  
399    an international key comparison exercise. This pilot study implies 12 NMI/DIs and is  
400    planned to be completed in 2022.

401    Meantime, the periodic quality control using toluene-based liquid scintillation sources of  
402     $^3\text{H}$  and  $^{14}\text{C}$  have been launched. They have permitted to demonstrate the capability of the  
403    ESIR to produce key comparison indicators with a good reproducibility for a 20-month  
404    period. This preliminary result is encouraging on the stability attainable by the unique  
405    method of the ESIR based on the TDCR technique.

406    Many challenges and perspectives are under study with ESIR such as,

- 407        • the adaptation of the source preparation facility to address alpha-emitting  
408        radionuclides (e.g.,  $^{211}\text{At}$ ,  $^{212}\text{Bi}$ ,  $^{212}\text{Pb}$ ,  $^{213}\text{Bi}$ ,  $^{227}\text{Th}$ ),
- 409        • the set-up of a redundant digital signal processing,
- 410        • the development of an LS cocktail prepared at the BIPM to allow on demand  
411        comparison for radionuclides emitting low energy particles (e.g.,  $^{55}\text{Fe}$ ,  $^{63}\text{Ni}$ ,  $^3\text{H}$   
412        and  $^{241}\text{Pu}$ ),

- 413       • the development of a transportable ESIR (analog to the SIRTI) using the  
414           transportable TDCR system developed by the LNE/LNHB [38].

415       **References**

- 416 [1]    CIPM 2003 Mutual recognition of national measurement standards and of  
417           calibration and measurement certificates issued by national metrology institutes
- 418 [2]    Karam L R 2007 Application of the CIPM MRA to radionuclide metrology  
419           *Metrologia* **44** 4–9
- 420 [3]    Rytz A 1983 The international reference system for activity measurements of  $\gamma$ -  
421           ray emitting nuclides *Int. J. Appl. Radiat. Isot.* **34** 1047–56
- 422 [4]    Ratel G 2007 The Système International de Référence and its application in key  
423           comparisons *Metrologia* **44** 7–16
- 424 [5]    Karam L, Judge S and Louw W 2019 The international measurement system for  
425           radionuclide metrology: A strategy for the future *Appl. Radiat. Isot.* **154** 108838
- 426 [6]    Michotte C, Nonis M, Bobin C, Altzizoglou T and Sibbens G 2013 *The SIRTI: a*  
427           *new tool developed at the BIPM for comparing activity measurements of short-*  
428           *lived radionuclides world-wide*
- 429 [7]    Coulon R, Courte S, Judge S, Michotte C and Nonis M 2021 Digitalization of the  
430           reporting of key comparisons for radionuclide metrology *Meas. Sci. Technol.*  
431           **Submitted** 113015
- 432 [8]    Sgouros G, Bodei L, McDevitt M R and Nedrow J R 2020 Radiopharmaceutical  
433           therapy in cancer: clinical advances and challenges *Nat. Rev. Drug Discov.* **19**  
434           589–608
- 435 [9]    Parker C, Lewington V, Shore N, Kratochwil C, Levy M, Lindén O, Noordzij W,  
436           Park J and Saad F 2018 Targeted Alpha Therapy, an Emerging Class of Cancer

- 437 Agents *JAMA Oncol.* **4** 1765
- 438 [10] Duchemin C, Ramos J P, Stora T, Ahmed E, Aubert E, Audouin N, Barbero E,  
439 Barozier V, Bernardes A-P, Bertreix P, Boscher A, Bruchertseifer F, Catherall R,  
440 Chevally E, Christodoulou P, Chrysalidis K, Cocolios T E, Comte J, Crepieux B,  
441 Deschamps M, Dockx K, Dorsival A, Fedosseev V N, Fernier P, Formento-  
442 Cavaier R, El Idrissi S, Ivanov P, Gadelshin V M, Gilardoni S, Grenard J-L,  
443 Haddad F, Heinke R, Juif B, Khalid U, Khan M, Köster U, Lambert L, Lilli G,  
444 Lunghi G, Marsh B A, Palenzuela Y M, Martins R, Marzari S, Menaa N, Michel  
445 N, Munos M, Pozzi F, Riccardi F, Riegert J, Riggaz N, Rinchet J-Y, Rothe S,  
446 Russell B, Saury C, Schneider T, Stegemann S, Talip Z, Theis C, Thiboud J, van  
447 der Meulen N P, van Stenis M, Vincke H, Vollaire J, Vuong N-T, Webster B,  
448 Wendt K and Wilkins S G 2021 CERN-MEDICIS: A Review Since  
449 Commissioning in 2017 *Front. Med.* **8**
- 450 [11] Iravani A, Violet J, Azad A and Hofman M S 2020 Lutetium-177 prostate-specific  
451 membrane antigen (PSMA) theranostics: practical nuances and intricacies *Prostate  
452 Cancer Prostatic Dis.* **23** 38–52
- 453 [12] Michotte C, Ratel G, Courte S, Johansson L, Keightley J, Arinc A, Bakhshandear  
454 E, Pommé S, Altzitzoglou T, Paepen J and Van Ammel R 2014 BIPM comparison  
455 BIPM.RI(II)-K1.Lu-177 of activity measurements of the radionuclide 177 Lu for  
456 the NPL (UK) and the IRMM (EU), with linked results for the comparison  
457 CCRI(II)-K2.Lu-177 *Metrologia* **51** 06002–06002
- 458 [13] Michotte C, Courte S, Nonis M, Coulon R, Judge S, Kossert K and Nähle O 2021  
459 Final report of the new BIPM comparison BIPM.RI(II)-K1.Ac-225 of activity  
460 measurements of the radionuclide 225 Ac to include the 2019 result of the PTB  
461 (Germany) *Metrologia* **58** 06018
- 462 [14] Michotte C, Courte S, Nonis M, Coulon R, Judge S, Ratel G, Fréchou C, Cassette  
463 P, Keightley J, Kossert K and Nähle O 2021 Final report of the new BIPM  
464 comparison BIPM.RI(II)-K1.Ra-223 of activity measurements of the radionuclide

- 465 223 Ra including the 2014 result of the NPL (United Kingdom), the 2014 result of  
466 the PTB (Germany) and the 2018 result of the LNE-LNHB (France) *Metrologia* **58**  
467 06007
- 468 [15] Wallenius M, Lützenkirchen K, Mayer K and Varga Z 2018 Actinides: Nuclear  
469 Forensics *Encyclopedia of Inorganic and Bioinorganic Chemistry* (Chichester,  
470 UK: John Wiley & Sons, Ltd) pp 1–17
- 471 [16] Jiang J, Davies A, Thorne K and Gilligan C 2017 Rapid analysis of <sup>89</sup>Sr and <sup>90</sup>Sr  
472 in nuclear forensics samples *J. Radioanal. Nucl. Chem.* **311** 1417–25
- 473 [17] Jiang J, Davies A V. and Britton R E 2017 Measurement of <sup>160</sup>Tb and <sup>161</sup>Tb in  
474 nuclear forensics samples *J. Radioanal. Nucl. Chem.* **314** 727–36
- 475 [18] Pochwalski K, Broda R and Radoszewski T 1988 Standardization of pure beta  
476 emitters by liquid-scintillation counting *Int. J. Radiat. Appl. Instrumentation. Part*  
477 **39** 165–72
- 478 [19] Broda R 2003 A review of the triple-to-double coincidence ratio (TDCR) method  
479 for standardizing radionuclides *Appl. Radiat. Isot.* **58** 585–94
- 480 [20] Nadjadi Y, Duc P F, Bochud F and Bailat C 2016 On the stability of <sup>3</sup>H and <sup>63</sup>Ni  
481 Ultima Gold liquid scintillation sources *Appl. Radiat. Isot.* **118** 25–31
- 482 [21] Coulon R, Broda R, Cassette P, Courte S, Jerome S, Judge S, Kossert K, Liu H,  
483 Michotte C and Nonis M 2020 The international reference system for pure β-  
484 particle emitting radionuclides: an investigation of the reproducibility of the results  
485 *Metrologia* **57** 035009
- 486 [22] Coulon R, Judge S, Liu H and Michotte C 2021 The international reference  
487 system for pure beta-particle emitting radionuclides: an evaluation of the  
488 measurement uncertainties *Metrologia* **58** 025007
- 489 [23] Kossert K, Sabot B, Cassette P, Coulon R and Liu H 2020 On the photomultiplier-  
490 tube asymmetry in TDCR systems *Appl. Radiat. Isot.* **163** 109223

- 491 [24] Broda R, Bonková I, Capogni M, Carconi P, Cassette P, Coulon R, Courte S,  
492 Felice P De, Dziel T, Fazio A, Frechou C, Galea R, García-Toraño E, Kołakowska  
493 E, Kossert K, Krivošík M, Lech E, Lee K B, Liang J, Listkowska A, Liu H,  
494 Navarro N, Nähle O J, Nowicka M, Rooy M van, Sabot B, Saganowski P, Sato Y,  
495 Tymiąski Z, Yunoki A, Zhang M and Ziemek T 2021 The CCRI(II)-K2.Fe-  
496 55.2019 key comparison of activity concentration measurements of a 55 Fe  
497 solution *Metrologia* **58** 06010
- 498 [25] EURAMET 2015 *Guidelines on the calibration of non-automatic weighing*  
499 *instruments*
- 500 [26] Lourenço V and Bobin C 2015 Weighing uncertainties in quantitative source  
501 preparation for radionuclide metrology *Metrologia* **52** S18–29
- 502 [27] Bobin C and Bouchard J 2006 A  $4\pi(\text{LS})\beta\text{-}\gamma$  coincidence system using a TDCR  
503 apparatus in the  $\beta$ -channel *Appl. Radiat. Isot.* **64** 124–30
- 504 [28] Cassette P and Do P 2008 The Compton source efficiency tracing method in  
505 liquid scintillation counting: A new standardization method using a TDCR counter  
506 with a Compton spectrometer *Appl. Radiat. Isot.* **66** 1026–32
- 507 [29] Anon ODM98-B
- 508 [30] Xiaoguang Zhong, Li Yu, Jiazhen Sun and Yuefang Zhang 1993 Radiation  
509 stability of PTFE irradiated under various conditions *Polym. Degrad. Stab.* **39**  
510 187–91
- 511 [31] Mitev K, Cassette P, Jordanov V, Liu H R and Dutsov C 2017 Design and  
512 performance of a miniature TDCR counting system *J. Radioanal. Nucl. Chem.* **314**  
513 583–9
- 514 [32] Jordanov V, Cassette P, Dutsov C and Mitev K 2020 Development and  
515 applications of a miniature TDCR acquisition system for in-situ radionuclide  
516 metrology *Nucl. Instruments Methods Phys. Res. Sect. A Accel. Spectrometers,*  
517 *Detect. Assoc. Equip.* **954** 161202

- 518 [33] Bouchard J and Cassette P 2000 MAC3: An electronic module for the processing  
519 of pulses delivered by a three photomultiplier liquid scintillation counting system  
520 *Appl. Radiat. Isot.* **52** 669–72
- 521 [34] Dutsov C, Cassette P, Sabot B and Mitev K 2020 Evaluation of the accidental  
522 coincidence counting rates in TDCR counting *Nucl. Instruments Methods Phys.*  
523 *Res. Sect. A Accel. Spectrometers, Detect. Assoc. Equip.* **977** 164292
- 524 [35] Michotte C, Courte S, Nonis M, Coulon R, Judge S, Nähle O and Takács M P  
525 2021 Update of the BIPM comparison BIPM.RI(II)-K1.Sr-85 of activity  
526 measurements of the radionuclide 85 Sr to include the 2018 result of the PTB  
527 (Germany) *Metrologia* **58** 06006
- 528 [36] Akgun U, Ayan A S, Aydın G, Duru F, Olson J and Onel Y 2008 Afterpulse  
529 timing and rate investigation of three different Hamamatsu Photomultiplier Tubes  
530 *J. Instrum.* **3** T01001–T01001
- 531 [37] Bobin C, Thiam C, Chauvenet B and Bouchard J 2012 On the stochastic  
532 dependence between photomultipliers in the TDCR method *Appl. Radiat. Isot.* **70**  
533 770–80
- 534 [38] Anon Discussion with Benoit Sabot, 2021  
535  
536

537

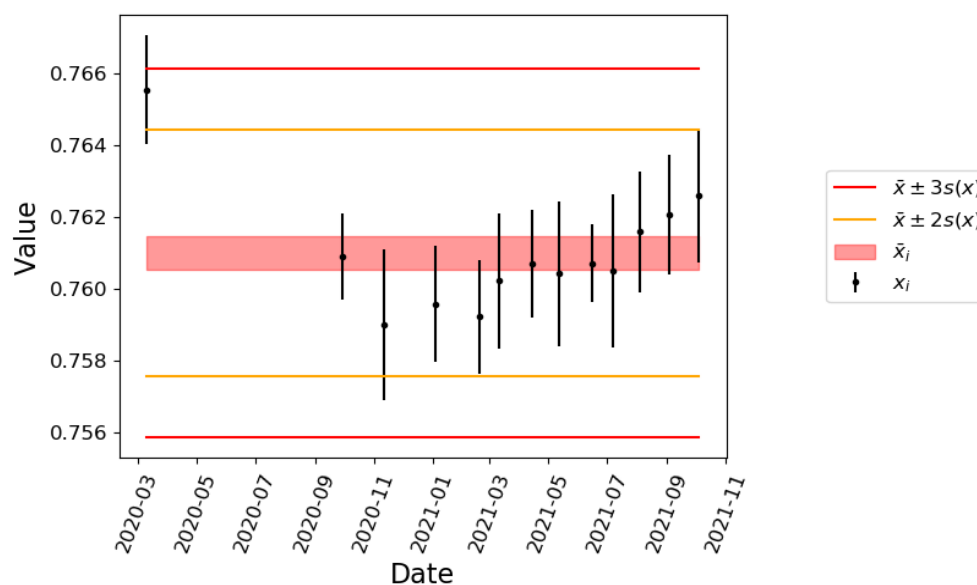
538

## Supplementary information

539 The full analysis of the period quality control is reported in this appendix. The error bars  
540 are standard uncertainty associate with the measurement points,  $x_i$ . The lower end upper  
541 control limits are the mean of all the measurement points  $\pm 2$  times (yellow lines) or 3  
542 times (red lines) standard deviation (type A evaluation). The central red line represents  
543 the mean with a thickness equal to  $\pm 1$  standard deviation of the mean value.

544

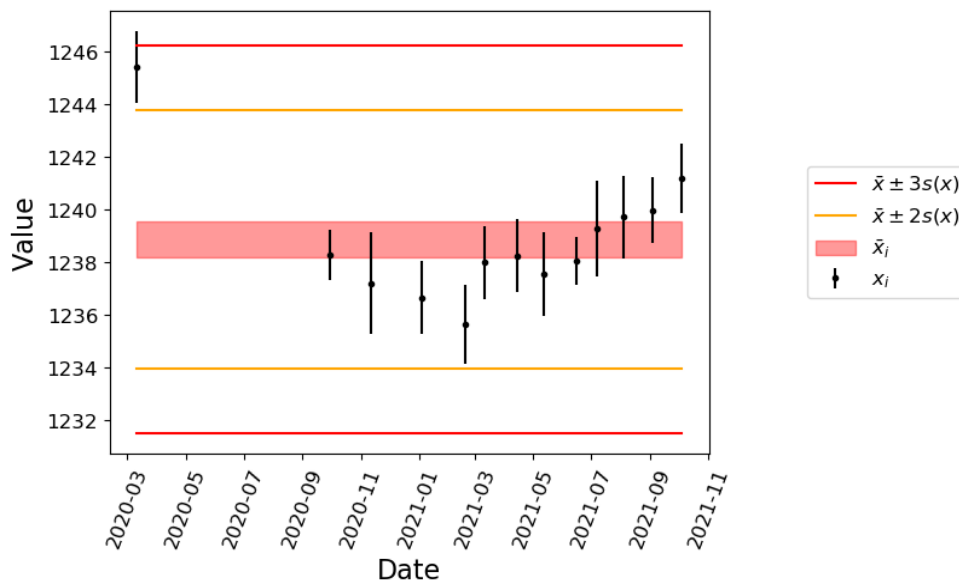
### a. Toluene-based tritium standard HDCO



545

546

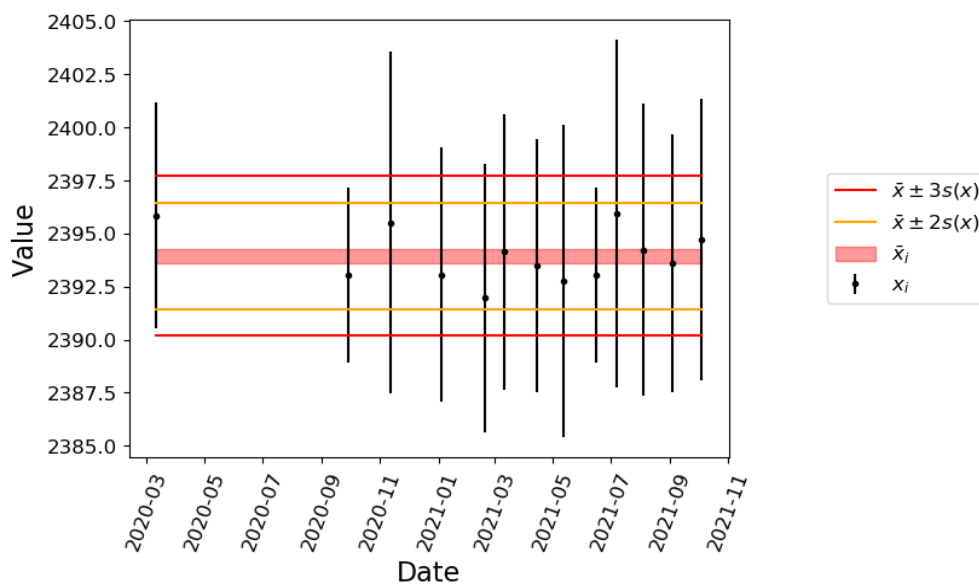
**Fig. 1** TDCR values obtained for the  $^3\text{H}$  source HDCO since March 2020



547

548

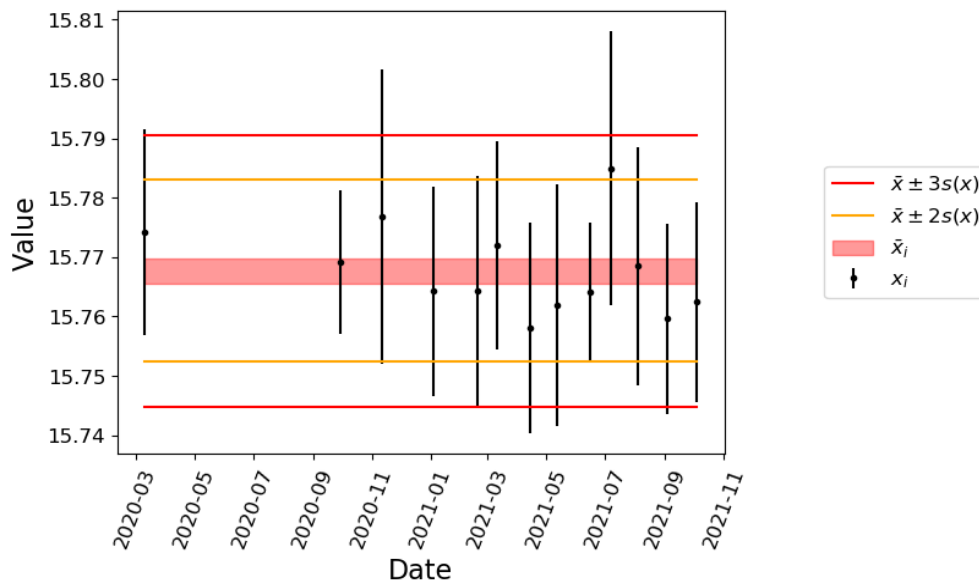
**Fig. 3**  $I_0$  values obtained for the  $^3\text{H}$  source HDCO since March 2020



549

550

**Fig. 2**  $I_1$  values obtained for the  $^3\text{H}$  source HDCO since March 2020



551

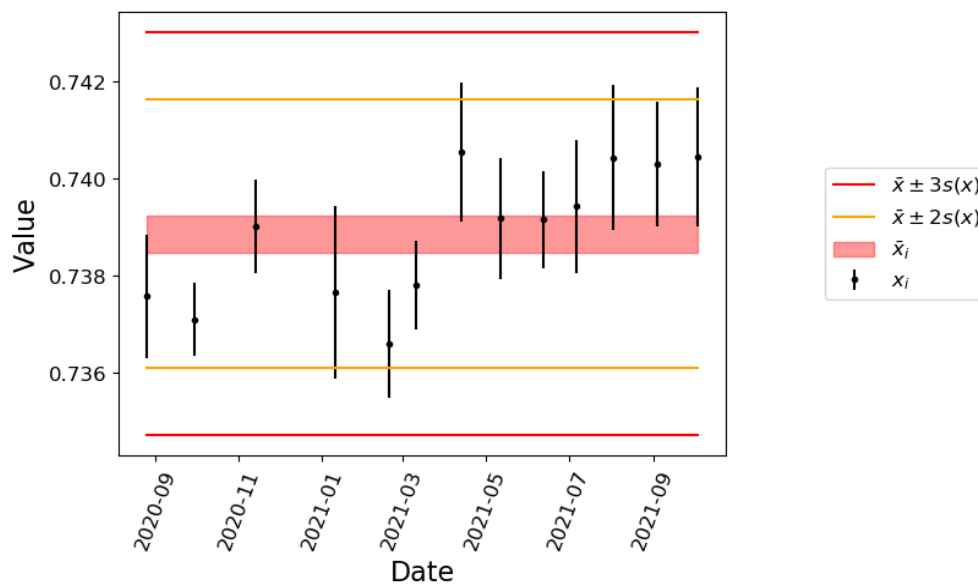
552

**Fig. 2**  $I_2$  values obtained for the  $^3\text{H}$  source HDCO since March 2020

553

554

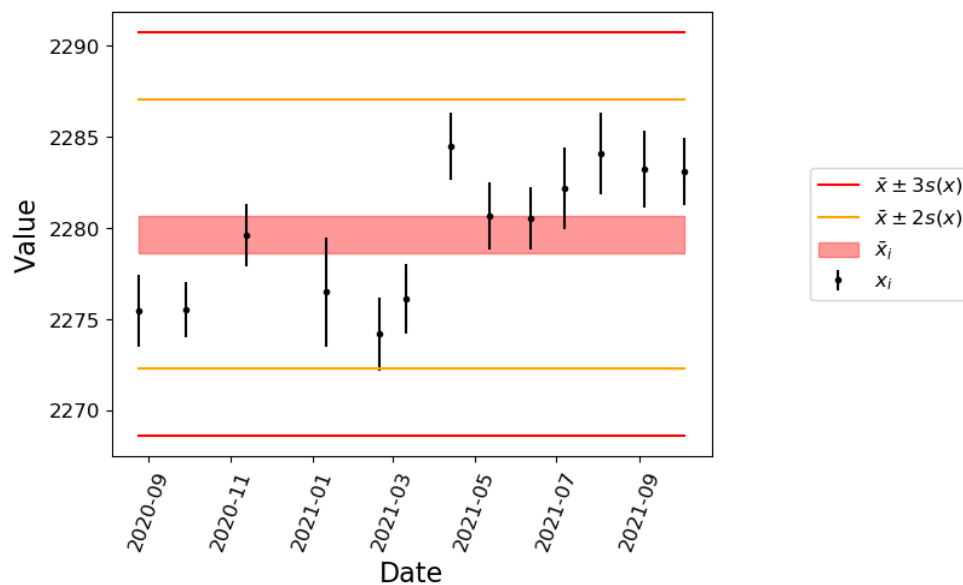
*b. Toluene-based tritium standard HMI*



555

556

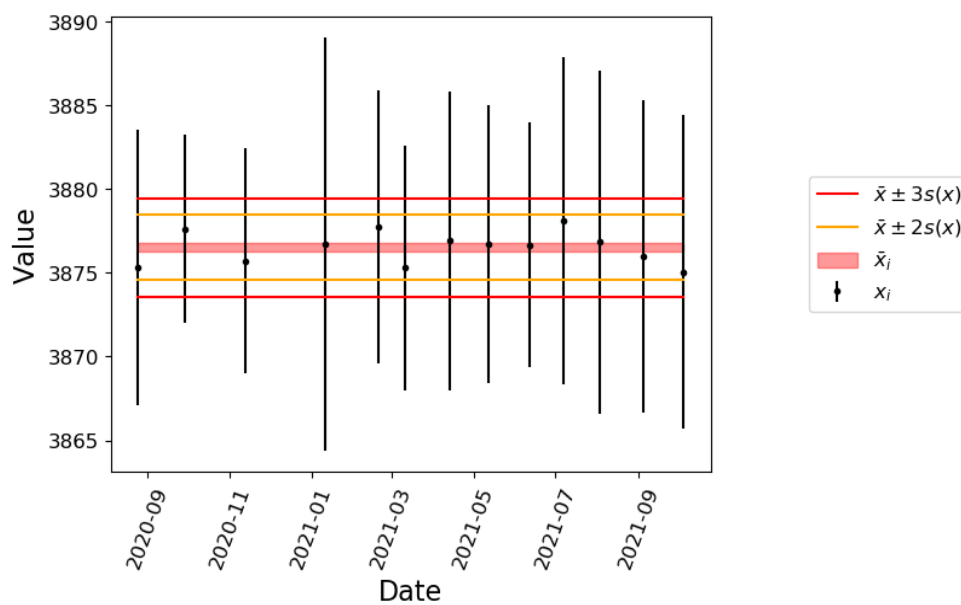
**Fig. 1** TDCR values obtained for the  $^3\text{H}$  source HMI since August 2020



557

558

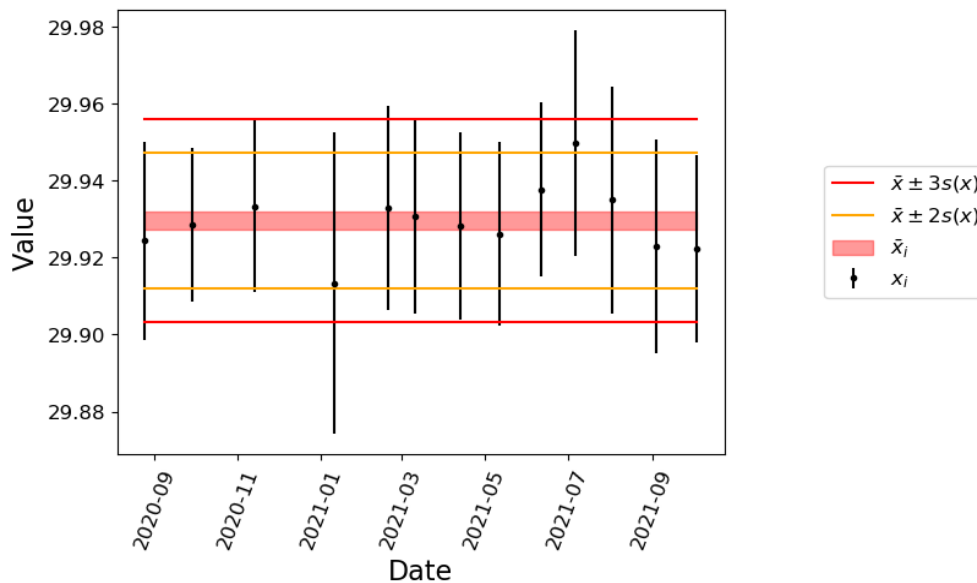
**Fig. 2**  $I_0$  values obtained for the  $^3\text{H}$  source HMI since August 2020



559

560

**Fig. 2**  $I_1$  values obtained for the  $^3\text{H}$  source HMI since August 2020



561

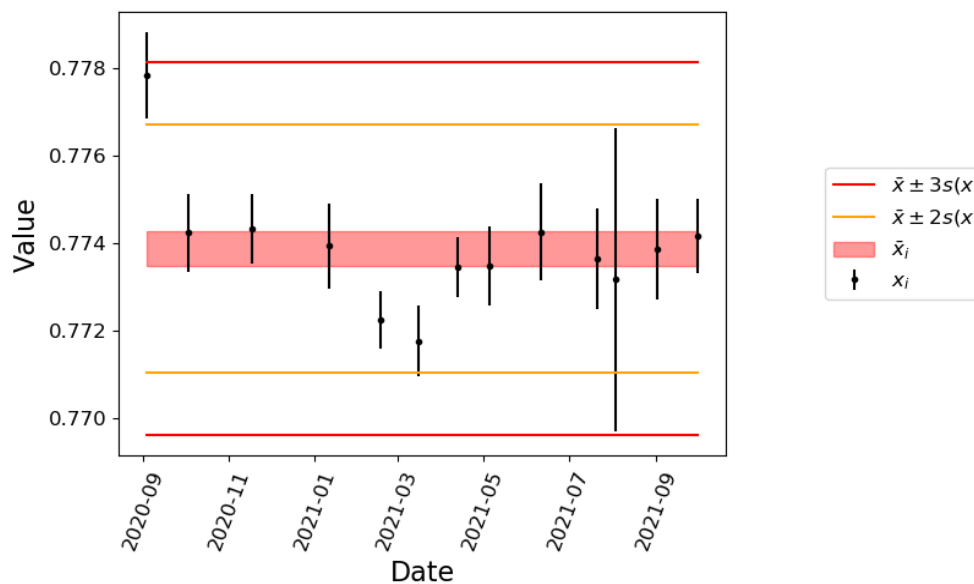
562

**Fig. 2**  $I_2$  values obtained for the  $^3\text{H}$  source HMI since August 2020

563

564

*c. Toluene-based tritium standard H3-117TOL*

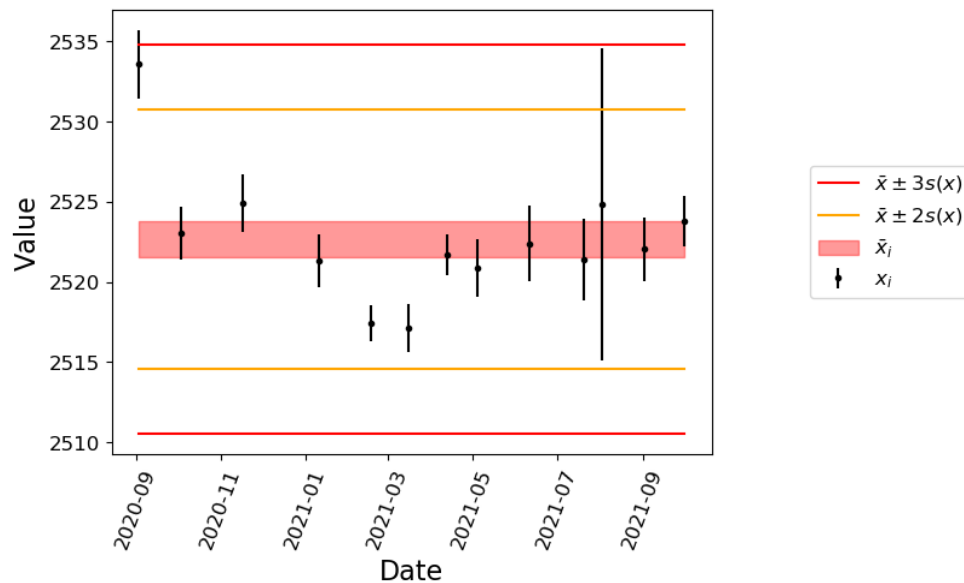


565

566

**Fig. 1** TDCR values obtained for the  $^3\text{H}$  source H3-117TOL since August 2020

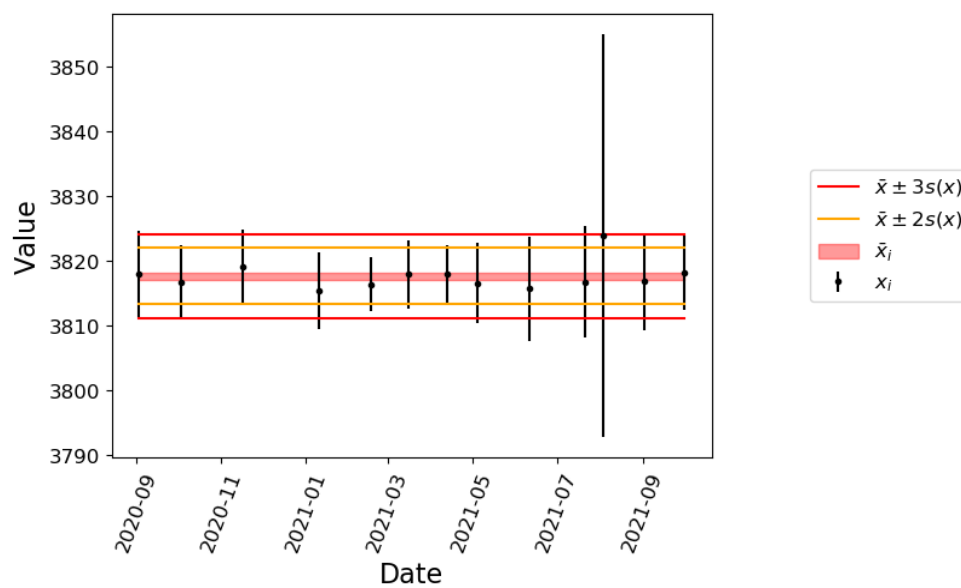
567



568

569

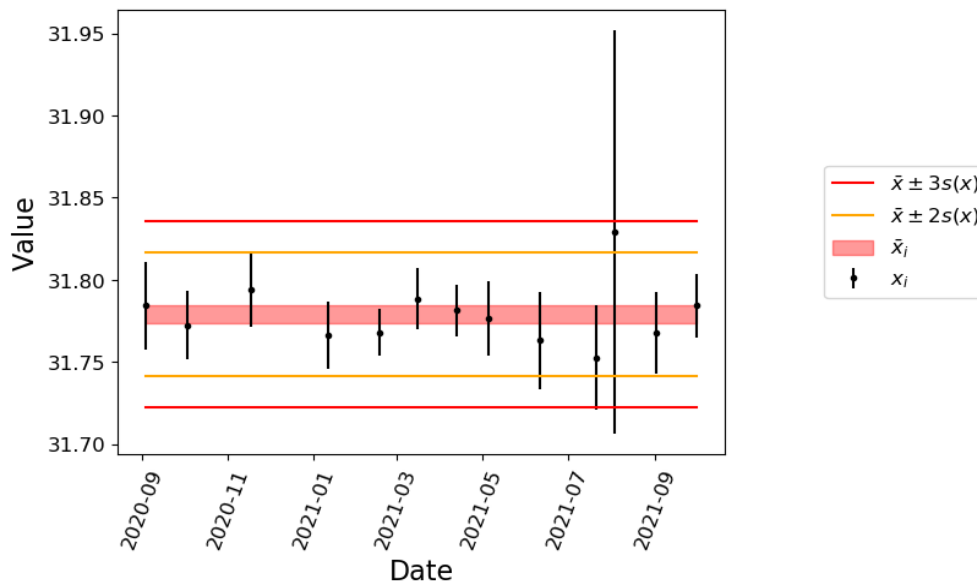
**Fig. 2**  $I_0$  values obtained for the  $^3\text{H}$  source H3-117TOL since August 2020



570

571

**Fig. 2**  $I_1$  values obtained for the  $^3\text{H}$  source H3-117TOL since August 2020



572

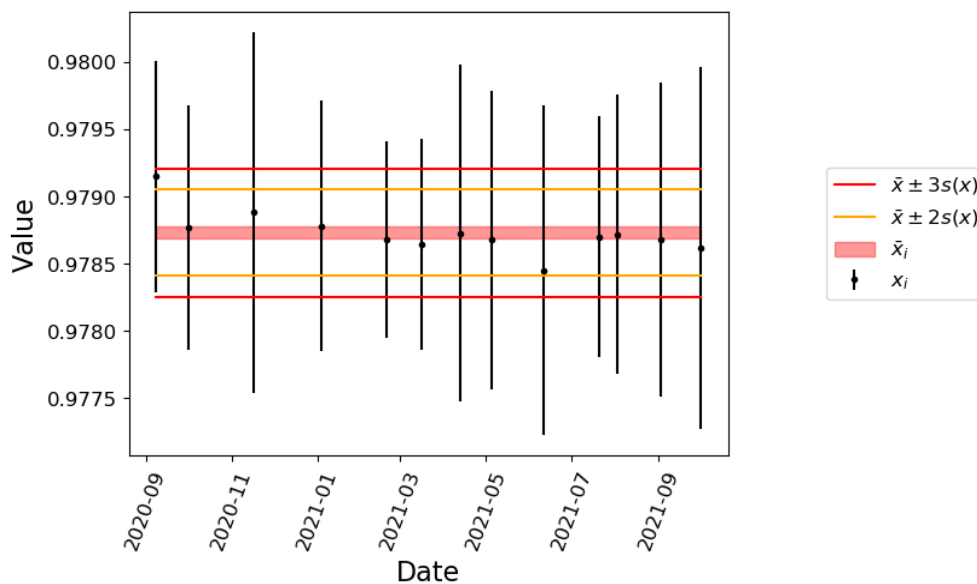
573

**Fig. 2**  $I_2$  values obtained for the  $^3\text{H}$  source H3-117TOL since August 2020

574

575

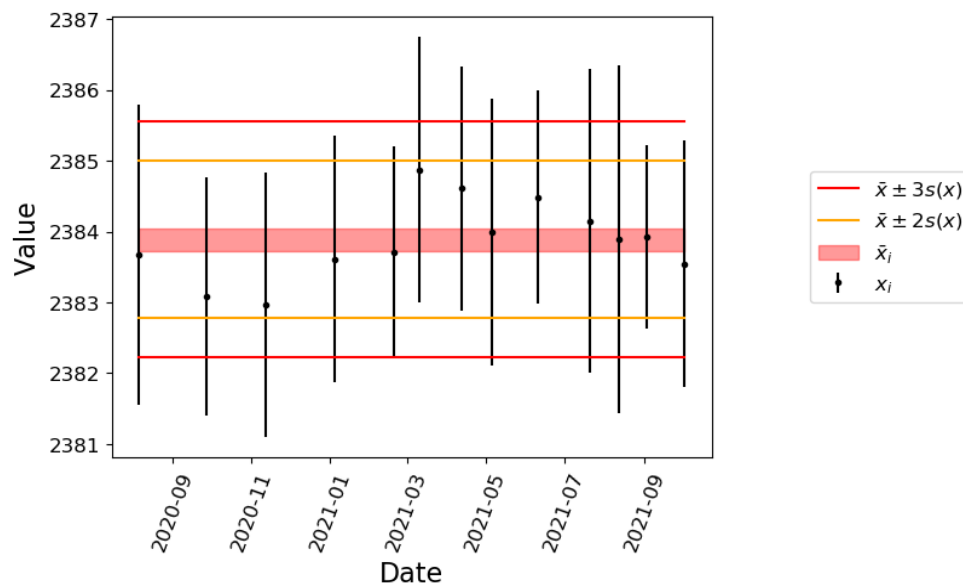
*d. Toluene-based  $^{14}\text{C}$  standard CCT*



576

577

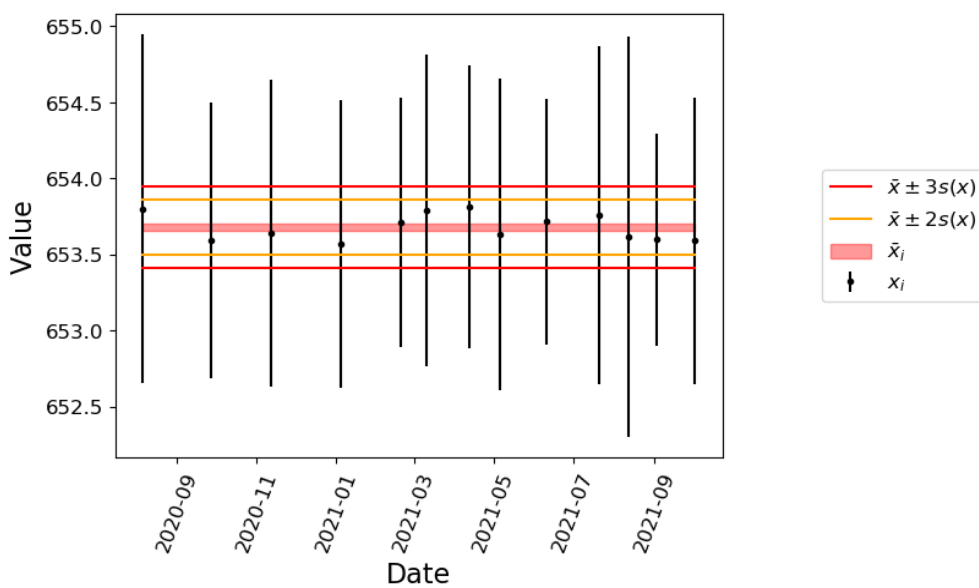
**Fig. 1** TDCR values obtained for the  $^{14}\text{C}$  source CCT since August 2020



578

579

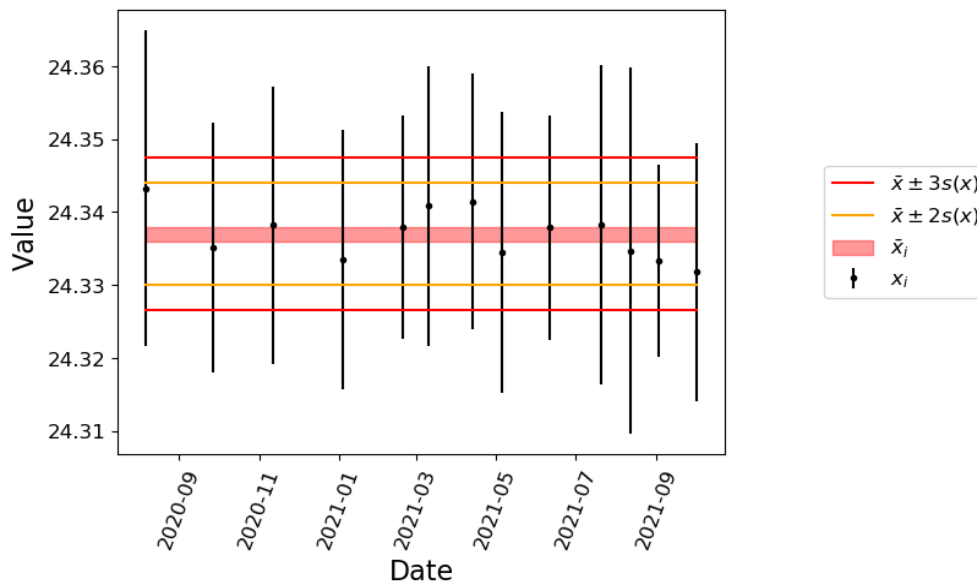
**Fig. 2**  $I_0$  values obtained for the  $^{14}\text{C}$  source CCT since August 2020



580

581

**Fig. 2**  $I_1$  values obtained for the  $^{14}\text{C}$  source CCT since August 2020



582

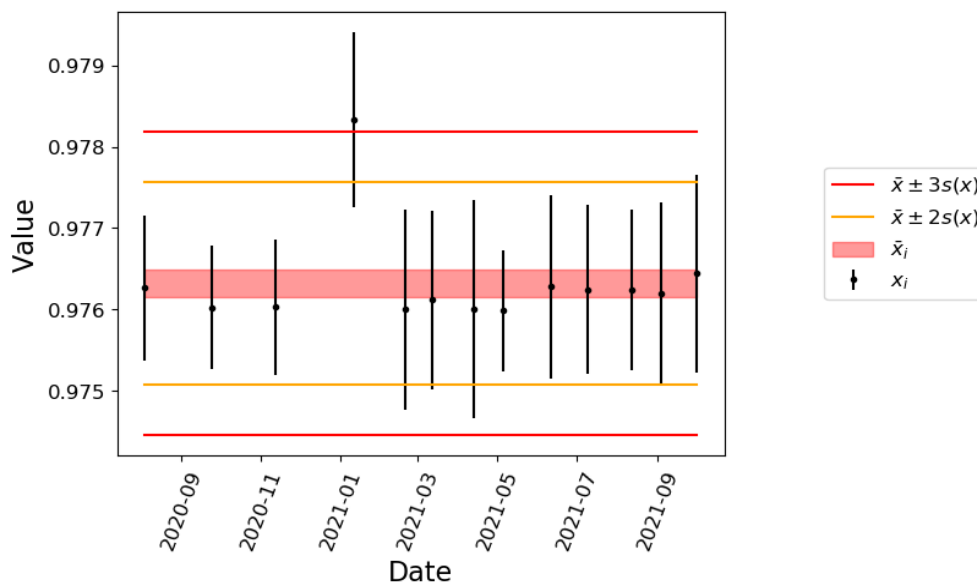
583

**Fig. 2**  $I_2$  values obtained for the  $^{14}\text{C}$  source CCT since August 2020

584

585

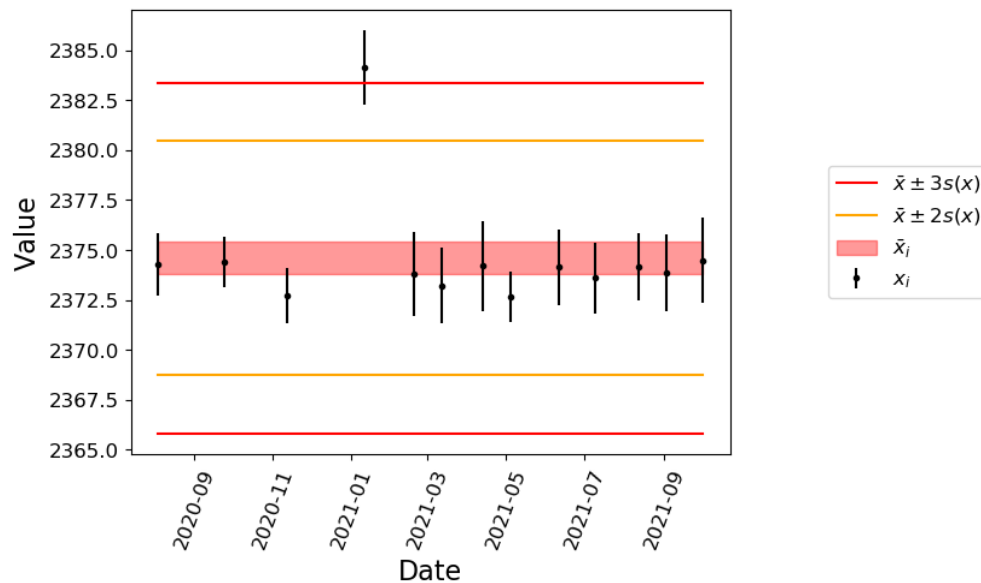
*e. Toluene-based  $^{14}\text{C}$  standard CMF*



586

587

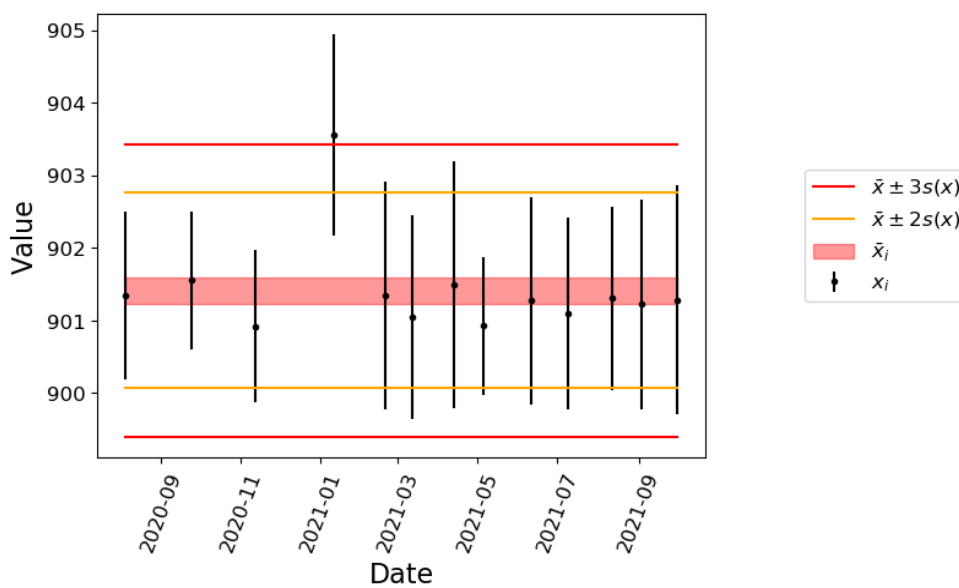
**Fig. 1** TDCR values obtained for the  $^{14}\text{C}$  source CMF since August 2020



588

589

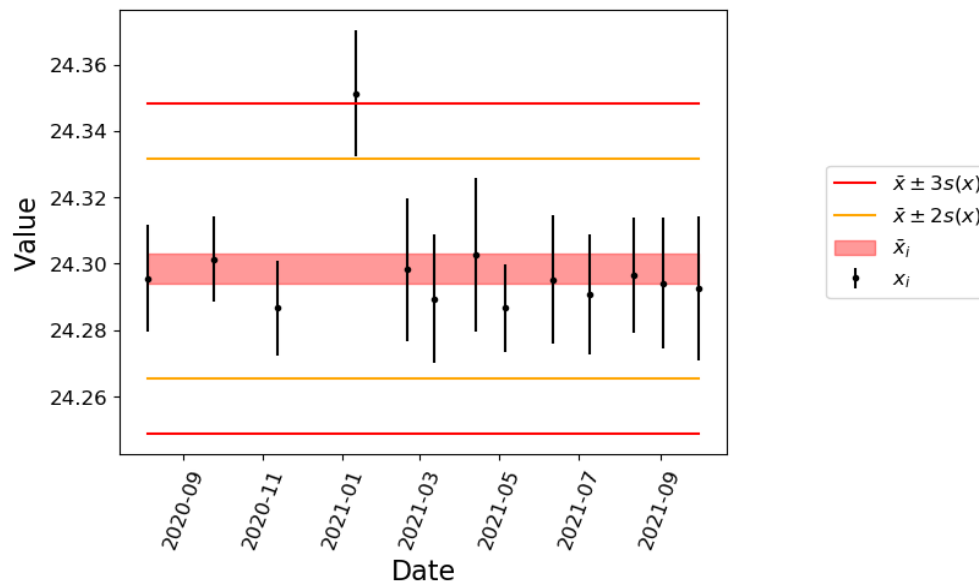
**Fig. 2**  $I_0$  values obtained for the  $^{14}\text{C}$  source CMF since August 2020



590

591

**Fig. 2**  $I_1$  values obtained for the  $^{14}\text{C}$  source CMF since August 2020



592

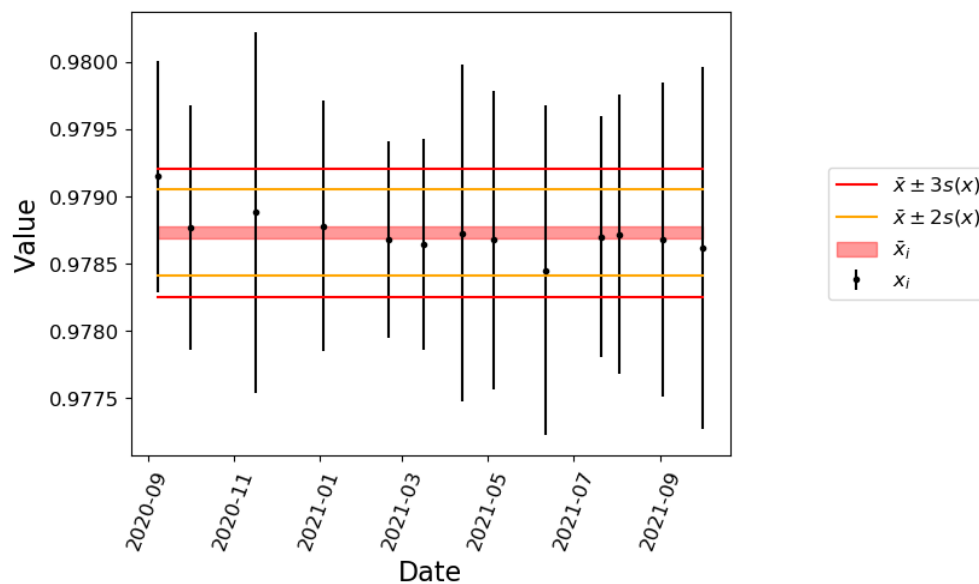
593

**Fig. 2**  $I_2$  values obtained for the  $^{14}\text{C}$  source CMF since August 2020

594

595

*f. Toluene-based  $^{14}\text{C}$  standard C14-117TOL*

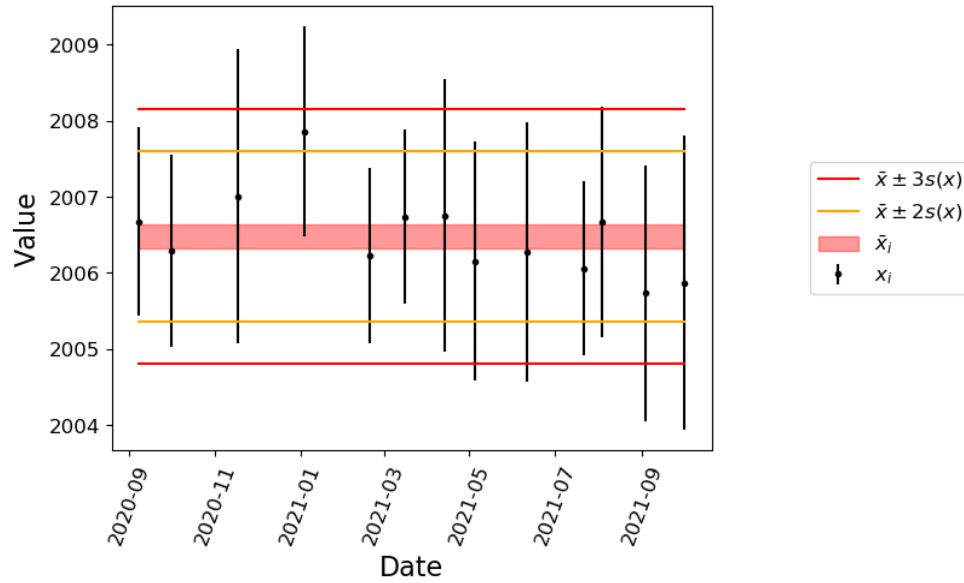


596

597

**Fig. 1** TDCR values obtained for the  $^{14}\text{C}$  source C14-117TOL since August 2020

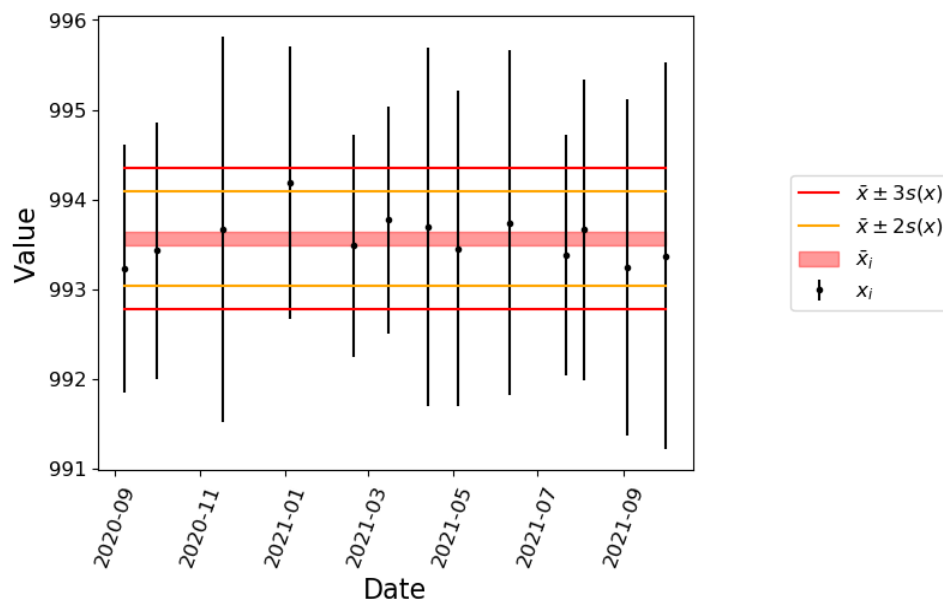
598



599

600

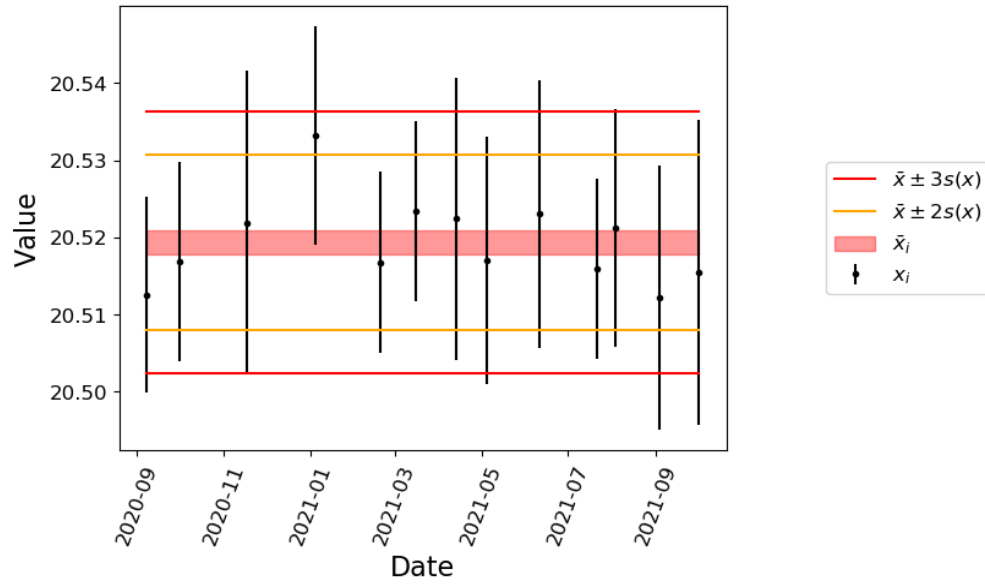
**Fig. 2**  $I_0$  values obtained for the  $^{14}\text{C}$  source C14-117TOL since August 2020



601

602

**Fig. 2**  $I_1$  values obtained for the  $^{14}\text{C}$  source C14-117TOL since August 2020



603

604

**Fig. 2**  $I_2$  values obtained for the  $^{14}\text{C}$  source C14-117TOL since August 2020

605